Decoupling of Axial Symmetric Three Antennas Based on Active Impedance Matching

Zhongyao Cao, *Graduate Student Member, IEEE*, Le Chang, *Senior Member, IEEE*, Yue Li, *Senior Member, IEEE*, Kunpeng Wei, *Senior Member, IEEE*, and Zhijun Zhang, *Fellow, IEEE*

***Abstract*— In this article, a novel decoupling scheme based on active impedance matching is proposed for the decoupling of axial symmetrical three antennas. Three simultaneous excitation modes with the same amplitude and different phase relationships are utilized to analyze the decoupling problem. In the perspective of simultaneous excitations, the decoupling of the three antenans can be transformed into active impedance matching. Theoretical demonstration reveals that achieving decoupling for axial symmetrical three antennas necessitates matching the active impedances under the three excitations. The active impedance matching can be solved intuitively in a clear step-by-step process by exploiting the impedance characteristics of the coupled three-line and the unique field distribution under different excitation modes. To validate the effectiveness of the proposed method, the decoupling of axial symmetric three inverted-F antennas (IFAs) is presented as an example. The achieved isolation exceeds 17 dB in the desired band with a peak isolation of 31 dB. With good isolation and a straightforward design process, the approach holds promise for future multi-input–multi-output (MIMO) antenna systems. Furthermore, the proposed method provides a new physical intuition for solving the decoupling problem of multiple antennas without the need for numerous optimizations.**

***Index Terms*— Active S-parameters, antenna decoupling, coupled three-line, lumped components.**

I. Introduction

THE application of multi-input–multi-output (MIMO) technique has proven to be an effective way of enhancing channel capacity. However, the mutual coupling between MIMO antennas poses a significant constraint on channel capacity improvement. In particular, the coupling between closely spaced antennas intensifies as the available space in modern equipment is progressively reduced. To address the issue of antenna decoupling, various schemes have been proposed in the past. Electromagnetic bandgap (EBG) [1], [2], [3] and defected ground structures (DGSs) [4], [5] operate by suppressing the propagation of coupled energy, thereby improving isolation. Neutralization line (NL) [6], [7], [8] and parasitic branches [9], [10], [11] introduce new coupled paths to cancel the original coupling. The isolation can be greatly enhanced when the coupled energy from different paths has the same amplitude and exhibits opposite phases. Based on the principle of coupled energy cancellation, the approaches incorporating metasurfaces [12], [13] and decoupling structures [14] to provide new coupling paths were proposed. For closely spaced antennas, approaches, such as self-multipath [15], shorted branches [16], and fence-strip resonator [17], have demonstrated good decoupling performances. Recently, the common mode and differential mode (CM/DM) decoupling method has been introduced [18], [19], [20], [21]. The method offers a more intuitive physical perspective on the decoupling problem without the demand for time-consuming tuning and iterative optimization. Based on the CM/DM theory, a wideband decoupling technique utilizing coupled co-planar waveguide (CPW) transmission lines was proposed in [22]. However, the CM/DM method is exclusively applicable to the decoupling of symmetrical antenna pairs.

The presence of multiple coupling paths between three antennas increases the complexity of decoupling. In the case of three antennas arranged with rotational symmetry, the coupling between any two ports is identical. Thus, the decoupling can be addressed by applying the solution derived from dual antenna decoupling through the insertion of a decoupling network [23]. However, the decoupling schemes for dual antennas cannot be extended to the decoupling of collinear symmetrically arranged three antennas. Different couplings between ports from asymmetric paths necessitate consideration and elimination. At a specific spacing, decoupling was achieved by adding only two bridge elements between adjacent antenna elements [24]. Another approach inserting dummy elements terminated with reactive loads realized high isolation between antennas [25]. A self-decoupling tri-port antenna is proposed, but the isolation of the antenna is only 11 dB [26]. Moreover, previous methods for decoupling of axial symmetric three antennas lack explicit design guidance based on physical meaning and thus require iteration and optimization.

In this article, a novel decoupling approach based on active impedance matching for axial symmetric three antennas is proposed with systematic design guidance. Based on the analysis

Manuscript received 29 November 2023; revised 8 May 2024; accepted 3 July 2024. Date of publication 18 July 2024; date of current version 9 September 2024. This work was supported in part by the National Natural Science Foundation of China under Contract 62271279. *(Corresponding author: Zhijun Zhang.)*

Zhongyao Cao, Yue Li, and Zhijun Zhang are with the Department of Electronic Engineering, Beijing National Research Center for Information Science and Technology, Tsinghua University, Beijing 100084, China (e-mail: zjzh@tsinghua.edu.cn).

Le Chang is with Shaanxi Key Laboratory of Deep Space Exploration Intelligent Information Technology, School of Information and Communications Engineering, Xi'an Jiaotong University, Xi'an 710049, China.

Kunpeng Wei is with Xiaomi Communications Company Ltd., Beijing 100085, China.

Color versions of one or more figures in this article are available at https://doi.org/10.1109/TAP.2024.3426977.

Digital Object Identifier 10.1109/TAP.2024.3426977

of the active reflection coefficient of port 1 under three different excitation modes, we transform the problem of antenna decoupling into the problem of active impedance matching. Utilizing the different active characteristic impedances of the coupled three-line, combined with the unique field distributions in mode 3, we can have two effective tools to match the active impedances. When the three active impedances are matched perfectly, ideal isolation between any two ports of the three passive antennas can be achieved. To validate the effectiveness of the proposed scheme, we take the decoupling of axial symmetric three inverted-F antennas (IFAs) as an example. The results illustrate that the proposed scheme can achieve good decoupling performance of collinear three antennas through a systematic, step-by-step process.

The remainder of this article is organized as follows. In Section II, the relationship between antenna decoupling and active impedance matching is analyzed. In Section III, the decoupling process of three IFAs is presented and discussed. In Section IV, the fabrication and measured performances are illustrated. Section V summarizes our work.

II. Principle of Decoupling Based on Active Reflection Coefficient

A. Analysis of Active S-Parameters

Active S-parameters containing information on mutual coupling are instructive for decoupling design. Under different excitation modes, the inconsistent active S-parameters character the properties of the mutual coupling between the antenna elements. In an array with m elements, the active reflection coefficient on the nth port under the excitation of Mode P with a specific combination of excitation amplitude and phase is [27]

$$S_{\mathrm{nn,Mode(P)}} = \frac{1}{a_{\mathrm{n}}} \sum_{\mathrm{k=1}}^{\mathrm{m}} S_{\mathrm{kn}} a_{\mathrm{k}} \tag{1}$$

where S_{kn} denotes the passive S-parameters of the m-port antenna array, and a_{k} denotes the input wave at the mth port. Fig. 1 shows arbitrary axial symmetric three antennas and the decoupling conditions between different ports. We analyze the decoupling of the three antennas by exciting them in three different modes, namely, Modes 1–3, with the same amplitude and different phase combinations. Exciting the three antennas simultaneously and observing the active S-parameters offer new physical insights into the decoupling problem. According to (1), in the excitation of the three different modes displayed in Fig. 1, the active S-parameters of port 1 are expressed as

$$S_{11,\mathrm{M1}} = S_{11} + S_{12} + S_{13} \tag{2}$$
$$S_{11,\mathrm{M2}} = S_{11} - S_{12} + S_{13} \tag{3}$$
$$S_{11,\mathrm{M3}} = S_{11} - S_{12} - S_{13} \tag{4}$$

where $S_{11,\mathrm{M1}}$, $S_{11,\mathrm{DM1}}$, and $S_{11,\mathrm{DM2}}$ are the active S-parameters of port 1 under Mode 1, Mode 2, and Mode 3 excitations, respectively. Then, by linear combination, we have

$$S_{12} = (S_{11,\mathrm{M1}} - S_{11,\mathrm{M2}})/2 \tag{5}$$
$$S_{13} = (S_{11,\mathrm{M2}} - S_{11,\mathrm{M3}})/2. \tag{6}$$

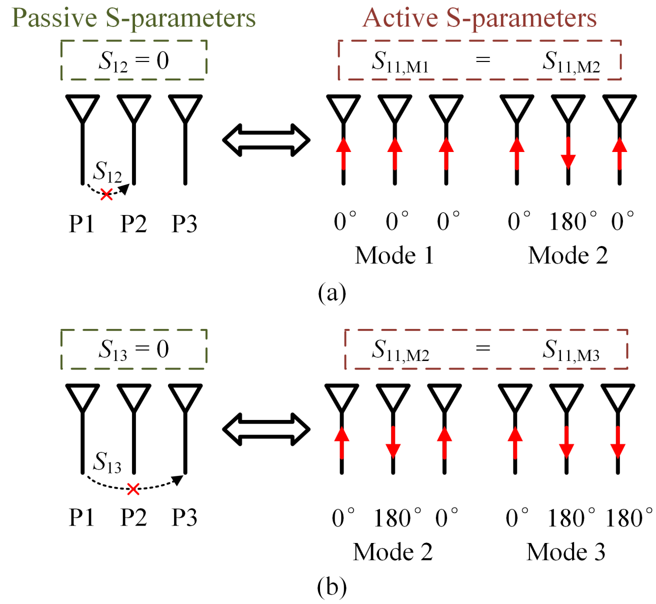

Fig. 1. Decoupling conditions for axial symmetrical three antennas. (a) Decoupling condition for ports 1 and 2. (b) Decoupling condition for ports 1 and 3.

For axial symmetric three antennas, we have $S_{11} = S_{33}$ and $S_{12} = S_{23}$. Decoupling aims are $S_{12} = S_{23} = 0$ and $S_{13} = 0$. In terms of (5) and (6), we can conclude that $S_{12} = 0$ is equivalent to $S_{11,\mathrm{M1}} = S_{11,\mathrm{M2}}$, and $S_{13} = 0$ is equivalent to $S_{11,\mathrm{M2}} = S_{11,\mathrm{M3}}$. With the premise that $S_{12} = S_{23}$, decoupling between any two ports can be attained when $S_{11,\mathrm{M1}} = S_{11,\mathrm{M2}} = S_{11,\mathrm{M3}}$, that is to say, the mutual coupling between any two ports can be eliminated when the active S-parameters of port 1 in three excitation modes are the same. Consequently, the decoupling problem can be transformed into the problem of active impedance matching.

Furthermore, the analysis of active impedance also reveals the properties of passive impedance matching. When ideal decoupling is achieved, the active reflection coefficient will be equal to the passive reflection coefficient. Therefore, if the three active impedances $Z_{11,\mathrm{M1}}$, $Z_{11,\mathrm{M2}}$, and $Z_{11,\mathrm{M3}}$ are matched to 50 Ω, i.e., $S_{11,\mathrm{M1}} = S_{11,\mathrm{M2}} = S_{11,\mathrm{M3}} = 0$, perfect passive impedance matching of ports 1 and 3 is also achieved. In this condition, only the impedance matching of port 2 is required to be accomplished. Based on the analysis of the active S-parameters, a systematic decoupling scheme by matching active impedances is proposed and analyzed in the following.

B. Decoupling Strategy

Based on the analysis above, for axial symmetric three antennas, decoupling can be transformed into the impedance matching of three active impedances $Z_{11,\mathrm{M1}}$, $Z_{11,\mathrm{M2}}$, and $Z_{11,\mathrm{M3}}$. In contrast to the decoupling problem, the impedance matching problem can be tackled in steps easily. A systematic decoupling strategy is presented in Fig. 2 with the use of coupled three-line and lumped components. In the adjusting process, once the former active impedance

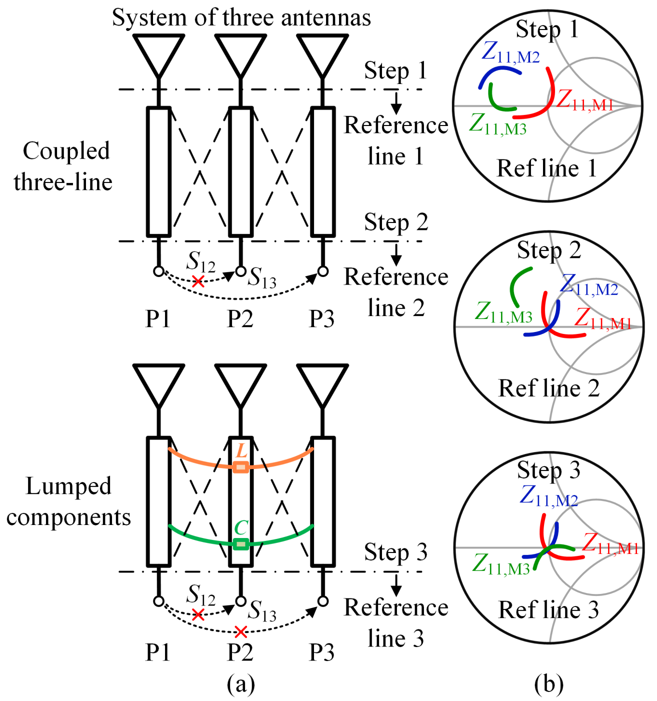

Fig. 2. Decoupling design procedure based on active impedance matching. (a) Structures introduced in the impedance matching steps with the corresponding decoupling results. (b) Active impedance loci in the Smith chart observed at three reference lines in three steps.

is matched, subsequent impedance matching operations do not alter the previous matching state. In the first step, we match $Z_{11,\mathrm{M1}}$ to 50 Ω without considering the other two active impedances. This step can be readily accomplished by adjusting the dimensions of each antenna, the characteristic impedance of the feeding line, and the values of lumped components in the matching circuit.

The second step is to match $Z_{11,\mathrm{M2}}$ without altering the matching state of $Z_{11,\mathrm{M1}}$. This can be achieved by adding a segment of coupled three-line, as shown in Fig. 2(a). The three active characteristic impedances of the coupled three-line under three excitations, i.e., $Z_{0,\mathrm{M1}}$, $Z_{0,\mathrm{M2}}$, and $Z_{0,\mathrm{M3}}$, deviate due to the mutual coupling among the lines. After adding a segment of coupled three-line, the three input active impedances observed at reference line 2 are

$$Z_{11,\mathrm{M1},r2} = Z_{0,\mathrm{M1}}\frac{Z_{11,\mathrm{M1},r1} + jZ_{0,\mathrm{M1}}\tan(\beta_{\mathrm{M1}}l)}{Z_{0,\mathrm{M1}} + jZ_{11,\mathrm{M1},r1}\tan(\beta_{\mathrm{M1}}l)} \quad (7)$$

$$Z_{11,\mathrm{M2},r2} = Z_{0,\mathrm{M2}}\frac{Z_{11,\mathrm{M2},r1} + jZ_{0,\mathrm{M2}}\tan(\beta_{\mathrm{M2}}l)}{Z_{0,\mathrm{M2}} + jZ_{11,\mathrm{M2},r1}\tan(\beta_{\mathrm{M2}}l)} \quad (8)$$

$$Z_{11,\mathrm{M3},r2} = Z_{0,\mathrm{M3}}\frac{Z_{11,\mathrm{M3},r1} + jZ_{0,\mathrm{M3}}\tan(\beta_{\mathrm{M3}}l)}{Z_{0,\mathrm{M3}} + jZ_{11,\mathrm{M3},r1}\tan(\beta_{\mathrm{M3}}l)} \quad (9)$$

where $Z_{11,\mathrm{M1,r2}}$, $Z_{11,\mathrm{M2,r2}}$, and $Z_{11,\mathrm{M3,r2}}$ are the input active impedances observed at reference line 2. $Z_{11,\mathrm{M1,r1}}$, $Z_{11,\mathrm{M2,r1}}$, and $Z_{11,\mathrm{M3,r1}}$ denote the input active impedance observed at reference line 1. $\beta_{\mathrm{MN}}l$ is the electric length of the coupled three-line of the Nth modes. Utilizing the inconsistent active characteristic impedances, the active impedances $Z_{11,\mathrm{M1}}$ and $Z_{11,\mathrm{M2}}$ can be manipulated separately. The matching state of $Z_{11,\mathrm{M1}}$ will not be altered when the active characteristic impedances $Z_{0,\mathrm{M1}}$ is designed to 50 Ω. By changing the linewidth and spacing of the coupled three-line, the active characteristic impedances $Z_{0,\mathrm{M2}}$ required to match $Z_{11,\mathrm{M2}}$ can be obtained while maintaining $Z_{0,\mathrm{M1}}$ at 50 Ω.

The third step involves matching $Z_{11,\mathrm{M3}}$ by loading two lumped components between the nonadjacent lines of the coupled three-line, as shown in Fig. 2(a). In Modes 1 and 2, as shown in Fig. 1(a), ports 1 and 3 are fed with the same amplitude and phase. The central plane can be equivalent to a perfect magnetic conductor (PMC) in the two modes. In contrast, in Mode 3, there is a potential difference between the nonadjacent two lines. Therefore, the added lumped components have no effect on $Z_{11,\mathrm{M1}}$ and $Z_{11,\mathrm{M2}}$ but alter $Z_{11,\mathrm{M3}}$. By adjusting the position and value of the loaded lumped components, the impedance $Z_{11,\mathrm{M3}}$ can be matched independently.

To help understand the design steps of the decoupling method, a design guideline is given as follows.

1) Extend the feeding line of ports 1 and 3 to the vicinity of port 2 to facilitate the following connections. Match the active impedance $Z_{11,\mathrm{M1}}$ by adjusting the antenna branches, feeding lines, and lumped components.
2) Adjust the linewidth and spacing of the coupled three-line to obtain the required $Z_{0,\mathrm{M2}}$ and keep $Z_{0,\mathrm{M1}}$ 50 Ω. Add the segment of coupled three-line to match $Z_{11,\mathrm{M2}}$ while keeping the matching state of $Z_{11,\mathrm{M1}}$ unchanged.
3) Add lumped components between the nonadjacent two lines of the coupled three-line to match $Z_{11,\mathrm{M3}}$ while keeping $Z_{11,\mathrm{M1}}$ and $Z_{11,\mathrm{M2}}$ constant.

To verify the feasibility of the proposed method, an example is analyzed and discussed in Section III.

III. Decoupling and Analysis of IFAs

In this section, the proposed decoupling strategy is applied to planar axial symmetric three IFAs. The widely used IFAs in modern wireless communication systems are chosen as an example. The proposed decoupling method can also be applied to other types of antennas. To guarantee symmetry of the structure, the three IFAs are required to be placed side by side. The original antenna configuration is depicted in Fig. 3, featuring three IFAs printed on a 1-mm FR-4 substrate. The initial mutual coupling is $|S_{12}| = |S_{23}| = -10$ dB and $|S_{13}| = -15$ dB, as shown in Fig. 3(b). The impedance loci of the three active impedances are presented in Fig. 3(c). Due to the high mutual coupling, the three impedance loci are away from each other on the Smith chart.

A. Active Impedance Matching of $Z_{11,M1}$

The antenna evolution and decoupling steps are summarized in Fig. 4. In Ant II, two transmission lines are included to facilitate the subsequent connection of the coupled three-line. From the perspective of mutual coupling, long transmission lines are necessary for the following circuits to provide additional coupling. The addition of transmission lines also provides an effective tool to match $Z_{11,\mathrm{M1}}$. As illustrated in Fig. 5, the transmission lines provide an effective means of adjusting active impedances. Incorporated with the adjustment of the

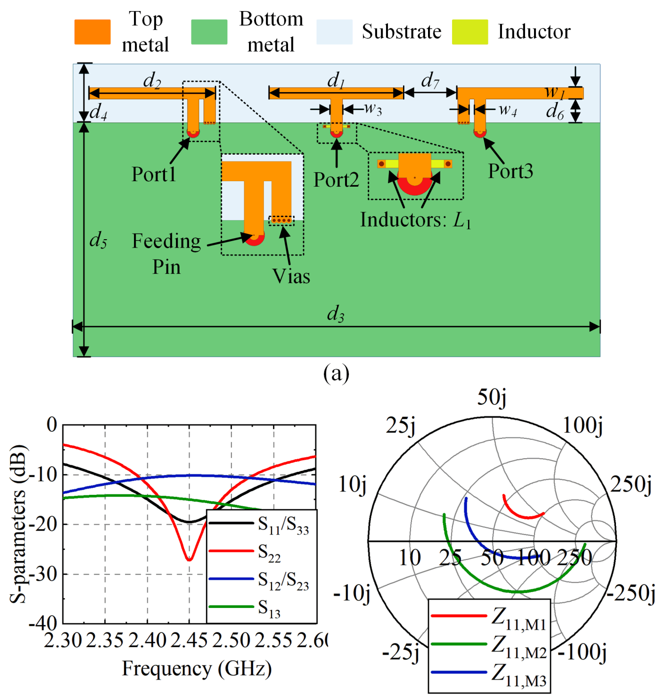

Fig. 3. (a) Configuration of the three IFAs. (b) S-parameters of the initial structure. (c) Impedance loci of three active impedances. The dimensions of Ant I are $d_1 = 20.2$, $d_2 = 20.7$, $d_3 = 90$, $d_4 = 10$, $d_5 = 40$, $d_6 = 4$, $d_7 = 10.6$, $w_1 = 2$, $w_3 = 2$, $w_4 = 1.2$, and $p = 0.1$, all in millimeters. The values of lumped components are $L_1 = 2.5$ nH.

dimensions of the antenna structure, $Z_{11,\mathrm{M1}}$ can be tuned to be near the matching point. The final dimensions of Ant II are summarized in Fig. 4. In Ant III, two capacitors are loaded on both sides of port 2 to connect the other two ports. As shown in Fig. 6, the loaded capacitors alter $Z_{11,\mathrm{M2}}$ and $Z_{11,\mathrm{M3}}$ in a wide range with less effect on $Z_{11,\mathrm{M1}}$. The addition of the capacitors facilitates the subsequent impedance matching with the coupled three-line. The reason that the capacitors have less effect on $Z_{11,\mathrm{M1}}$ is that only a small amount of current flows through the capacitors when all ports are fed in-phase in Mode 1. In contrast, in the case of out-of-phase feeding in Modes 2 and 3, the capacitor has a more pronounced effect on the active impedances.

B. Active Impedance Matching of $Z_{11,M2}$

A segment of coupled three-line with a length of L_m is introduced to match $Z_{11,\mathrm{M2}}$ to 50 Ω while maintaining the matching state of $Z_{11,\mathrm{M1}}$ unchanged in Ant IV. The characteristic modes of the coupled three-line are analyzed in [28]. Instead of utilizing the characteristic mode impedance, we analyze the active characteristic impedance of the coupled three-line under different feeding modes. The active characteristic impedances can be manipulated by adjusting the linewidth and spacing of the coupled three-line. The effect of the linewidth and spacing of the coupled three-line on active characteristic impedance is displayed in Fig. 7. The line spacing s alters the coupling between the three lines. As depicted in Fig. 7(a), with an increase in line spacing s, the impedances $Z_{0,\mathrm{M1}}$ and

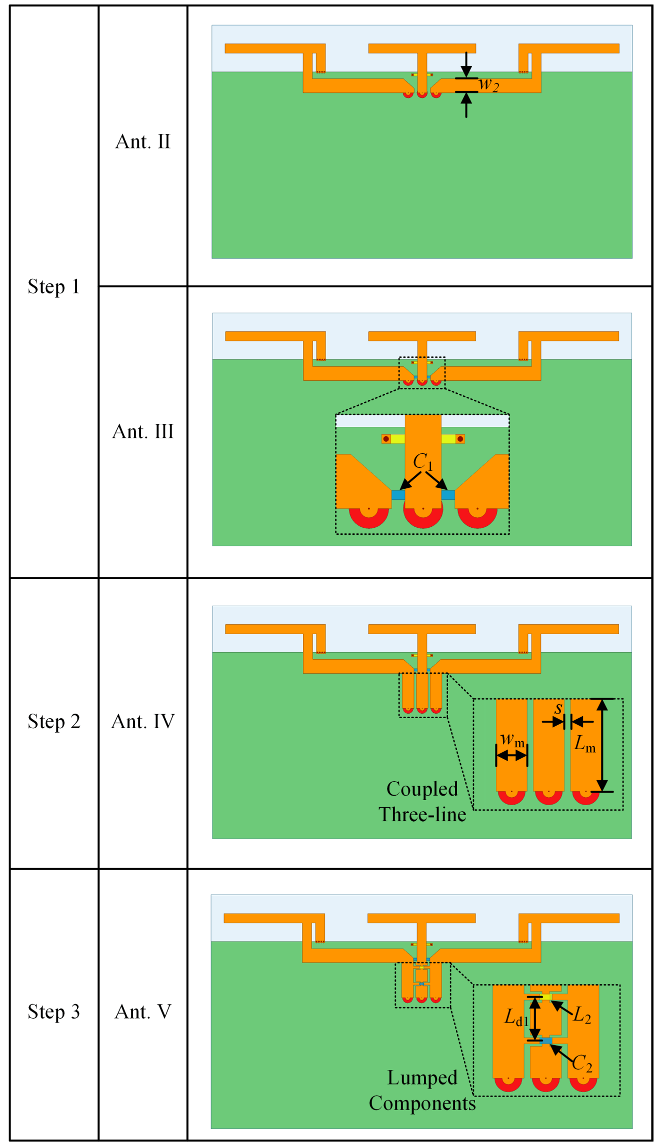

Fig. 4. Design process of the proposed antenna.

$Z_{0,\mathrm{M2}}$ become closer due to the weakened coupling. All the active characteristic impedances decrease as the linewidth w_m decreases, as shown in Fig. 7(b). Thus, by varying s and w_m, the desired combination of active characteristic impedances $Z_{0,\mathrm{M1}}$ and $Z_{0,\mathrm{M2}}$ can be easily obtained. Finally, in Ant IV, the dimensions of the coupled three-line are chosen as $s = 0.5$ mm and $w_\mathrm{m} = 2.5$ mm. The simulated active characteristic impedances $Z_{0,\mathrm{CM}}$, $Z_{0,\mathrm{M2}}$, and $Z_{0,\mathrm{M3}}$ under the specific parameters are 48.9 Ω (≈50 Ω), 34.3 Ω, and 32.1 Ω, respectively.

In Fig. 8(a)–(c), the three active impedances $Z_{11,\mathrm{M1}}$, $Z_{11,\mathrm{M2}}$, and $Z_{11,\mathrm{M3}}$ are presented in the Smith charts with different lengths of the coupled three-line L_m. When provided with an active characteristic impedance $Z_{0,\mathrm{M1}}$ close to 50 Ω, the input active impedance $Z_{11,\mathrm{M1}}$ exclusively rotates along a point close to the center of the Smith chart, as shown in Fig. 8(a). Consequently, for any length of the coupled three-line, the matching state of $Z_{11,\mathrm{M1}}$ remains unchanged. Fig. 8(b) and (c) depicts the variation of the other two active impedances. As the

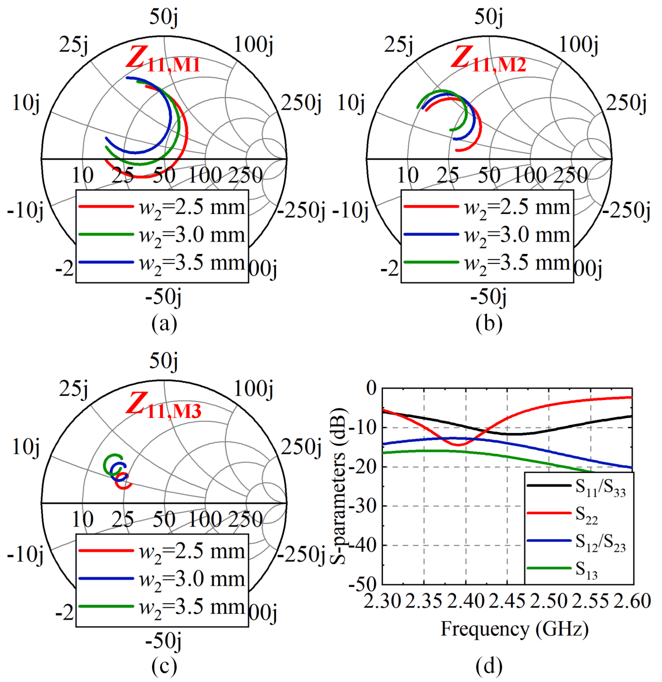

Fig. 5. Impedance loci on Smith chart of (a) $Z_{11,\mathrm{M1}}$, (b) $Z_{11,\mathrm{M2}}$, and (c) $Z_{11,\mathrm{M3}}$ of Ant II. (d) S-parameters of Ant II. The final dimensions of Ant II are $d_1 = 23$, $d_2 = 21.5$, $d_3 = 90$, $d_4 = 10$, $d_5 = 40$, $d_6 = 4$, $d_7 = 9.2$, $w_1 = 2$, $w_2 = 2.5$, $w_3 = 2$, $w_4 = 1.2$, and $p = 0.1$, all in millimeters. The final values of lumped components are $L_1 = 1.6$ nH.

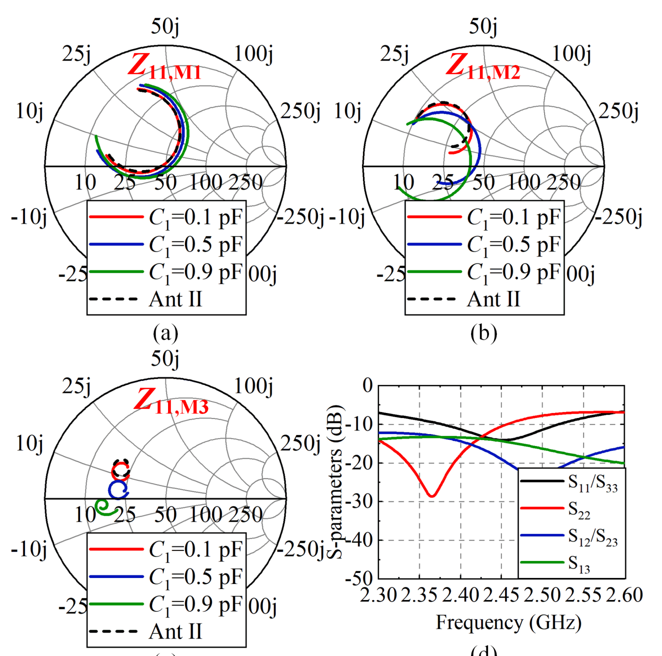

Fig. 6. Impedance loci on Smith chart of (a) $Z_{11,\mathrm{M1}}$, (b) $Z_{11,\mathrm{M2}}$, and (c) $Z_{11,\mathrm{M3}}$ of Ant III. (d) S-parameters of Ant III. The final dimensions of Ant III are $d_1 = 23$, $d_2 = 21.5$, $d_3 = 90$, $d_4 = 10$, $d_5 = 40$, $d_6 = 4$, $d_7 = 9.2$, $w_1 = 2$, $w_2 = 2.5$, $w_3 = 2$, $w_4 = 1.2$, and $p = 0.1$, all in millimeters. The values of lumped components are $L_1 = 2.5$ nH and $C_1 = 0.5$ pF.

length L_m increases from 4 to 12 mm with a 3-mm increment, the active impedances $Z_{11,\mathrm{M2}}$ and $Z_{11,\mathrm{M3}}$ are adjusted according to their respective active characteristic impedances. When the length of the coupled three-line L_m is 9 mm, the active

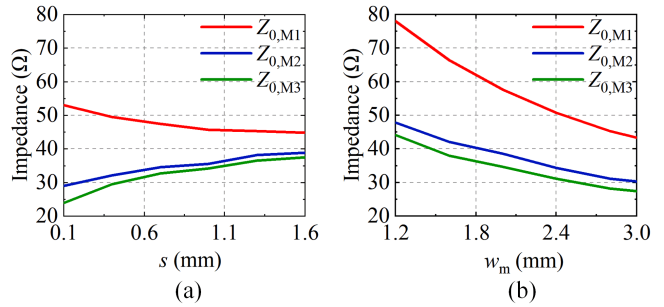

Fig. 7. Characteristic active impedance of port 1 of the coupled three-line with different (a) line spacings s and (b) linewidths w_m.

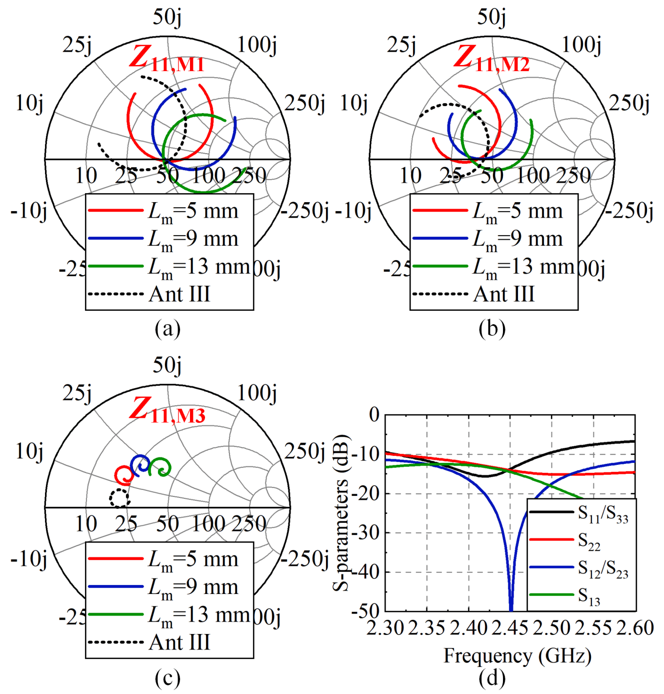

Fig. 8. Impedance loci on Smith chart of (a) $Z_{11,\mathrm{M1}}$, (b) $Z_{11,\mathrm{M2}}$, and (c) $Z_{11,\mathrm{M3}}$ in Ant IV with different lengths of coupled three-line. (d) S-parameters of Ant IV. The final dimensions of Ant IV are $d_1 = 23$, $d_2 = 21.5$, $d_3 = 90$, $d_4 = 10$, $d_5 = 40$, $d_6 = 4$, $d_7 = 9.2$, $w_1 = 2$, $w_2 = 2.5$, $w_3 = 2$, $w_4 = 1.2$, $p = 0.1$, and $L_m = 9$, all in millimeters. The values of lumped components are $L_1 = 2.5$ nH and $C_1 = 0.5$ pF.

impedance $Z_{11,\mathrm{M2}}$ can be matched to 50 Ω. At this point, the mutual coupling $|S_{12}|/|S_{23}|$ is significantly improved, as shown in Fig. 8(d).

C. Active Impedance Matching of $Z_{11,M3}$

Finally, lumped components are introduced between the two lines to match $Z_{11,\mathrm{M3}}$ to 50 Ω independently in Ant V. The electric field distributions at 2.45 GHz under three excitation modes are shown in Fig. 9. As analyzed before, under Mode 1 and Mode 2 excitation, the symmetry plane of the structure can be equivalent to a virtual PMC boundary. However, under Mode 3 excitation, no clear boundary exists in the symmetry plane due to the asymmetry feeding phase. The inconsistency in the equivalent boundary on the symmetry plane is the basis for achieving independent impedance matching of $Z_{11,\mathrm{M3}}$. The PMC boundary can be regarded as an open circuit, so the

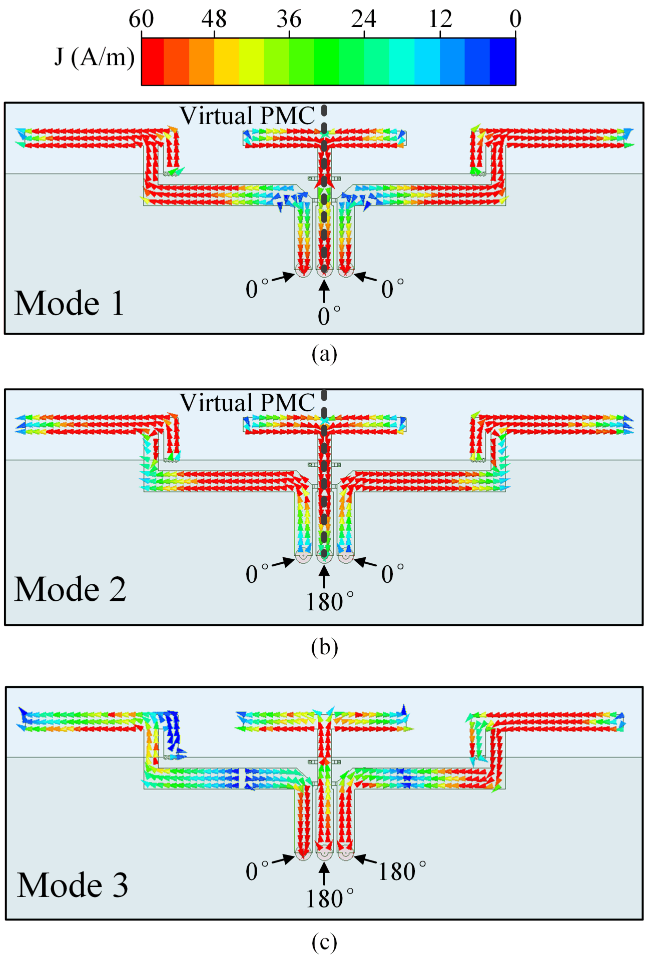

Fig. 9. Vector current distribution under three feeding modes of Ant IV at 2.45 GHz. (a) Mode 1 excitation. (b) Mode 2 excitation. (c) Mode 3 excitation.

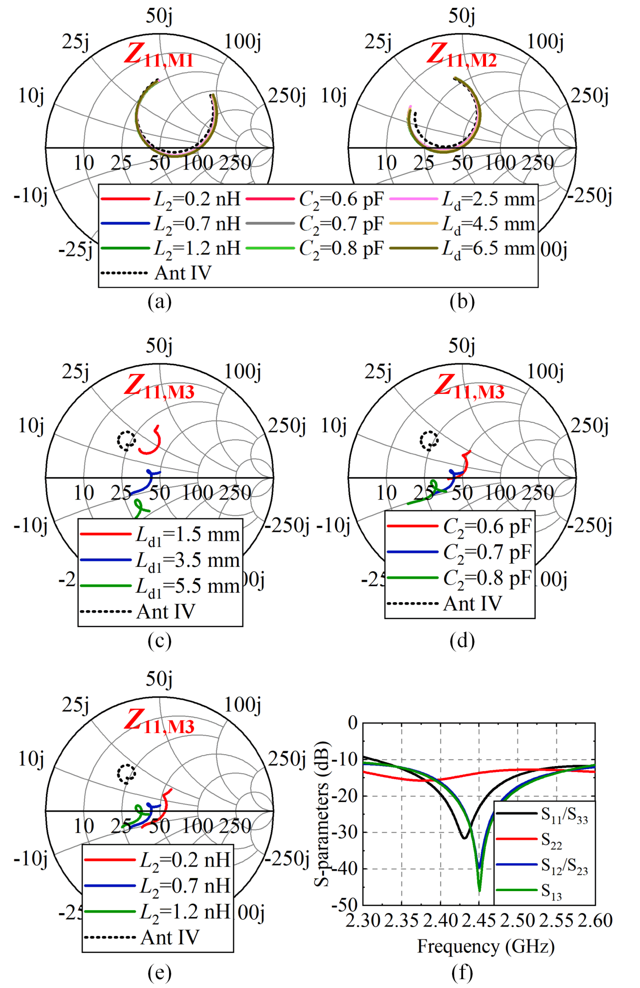

Fig. 10. Impedance loci on Smith chart of (a) $z_{11,M1}$, (b) $z_{11,M2}$, (c) $z_{11,M3}$, (d) $z_{11,M3}$, and (e) $Z_{11,M3}$ in Ant V with different values of capacitors and inductors. (e) S-parameters of Ant V. The final dimensions of Ant V are $d_1 = 23$, $d_2 = 21.5$, $d_3 = 90$, $d_4 = 10$, $d_5 = 40$, $d_6 = 4$, $d_7 = 9.2$, $w_1 = 2$, $w_2 = 2.5$, $w_3 = 2$, $w_4 = 1.2$, $p = 0.1$, $L_m = 7.5$, and $L_{d1} = 4.5$, all in millimeters. The values of lumped components are $L_1 = 2.5$ nH, $C_1 = 0.5$ pF, $L_2 = 0.7$ nH, and $C_2 = 0.7$ pF.

lumped components across the boundary have no effect on the current distribution and the active impedances. In contrast, as a potential difference exists between ports 1 and 3, current flows through the lumped components added in the middle. Consequently, the active impedance $Z_{11,M3}$ can be manipulated independently with the addition of lumped components.

Considering the physical package size of the lumped components, in Ant V, slight modifications are made to the coupled three-line to facilitate soldering. Two small portions of the center line are narrowed and the outer two lines are partially extended toward the center, as displayed in Fig. 4. The change in linewidth introduces alterations in active characteristic impedances. However, the portion of the line with adjusted width has a short electrical length, and thus, the alteration of the input active impedance is limited. To compensate for the slight changes in $Z_{11,M1}$ and $Z_{11,M2}$, the length of the coupled three-line L_m is adjusted to 7.5 mm in Ant V while keeping other dimensions constant. The impedance loci on the Smith chart are illustrated in Fig. 10(a)–(e). In the figure, L_m in Ant IV is also adjusted to 7.5 mm to better demonstrate the change in the three active impedances with the addition of lumped components. As displayed in Fig. 10(a) and (b), the variation in inductor L_2, capacitor C_2, and the distance between the two lumped components L_{d1} has a negligible effect on $Z_{11,M1}$ and $Z_{11,M2}$. The slight change in impedance from Ant IV to Ant V is attributed to the altered width of the coupled three-line. As illustrated in Fig. 10(c)–(e), we can adjust the value of inductor L_2, capacitor C_2, and the distance between the two lumped components L_{d1} to match $Z_{11,M3}$ independently.

Finally, in Ant V all the three active impedances $Z_{11,M1}$, $Z_{11,M2}$, and $Z_{11,M3}$ are tuned to 50 Ω at the desired band with $L_2 = 0.7$ nH, $C_2 = 0.7$ pF, and $L_{d1} = 3.5$ mm. As analyzed before, when the condition of $S_{11,M1} = S_{11,M2} = S_{11,M3}$ is attained, the mutual coupling between any two ports can be eliminated, as presented in Fig. 10(f). Moreover, the matched three active impedances imply good passive impedance matching of ports 1 and 3. In Ant V, acceptable impedance matching of port 2 is naturally achieved and an additional circuit is not required. If the impedance matching of port 2 is unsatisfactory, lumped components can be introduced for impedance matching, which can be realized easily after the elimination of mutual coupling.

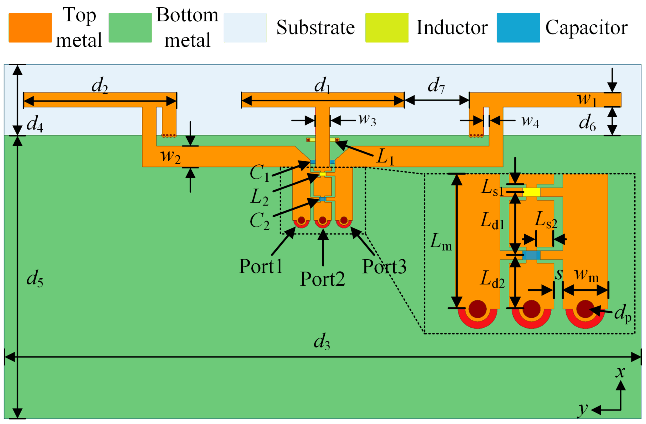

Fig. 11. Configuration of the proposed antenna.

TABLE I
DETAILED DIMENSIONS OF THE PROPOSED ANTENNA

Parameter	Value (mm)	Parameter	Value (mm)
d_1	23	w_4	0.8
d_2	21.5	w_m	2.5
d_3	90	L_m	7.5
d_4	10	L_{d1}	3.5
d_5	40	L_{d2}	3
d_6	4	L_{s1}	0.45
d_7	9.2	L_{s2}	0.95
w_1	2	s	0.5
w_2	3	d_p	1
w_3	2		

IV. CONFIGURATION AND RESULTS

A. Antenna Configuration

The final configuration of the proposed antenna is shown in Fig. 11. A ground size of 40 × 90 mm with three IFAs is printed on both sides of an FR-4 substrate ($\varepsilon_r = 4.4$ and $\tan\delta = 0.02$) with a thickness of 1 mm. The detailed dimensions are displayed in Table I. The final values of the lumped components are $L_1 = 1.6$ nH, $C_1 = 0.5$ pF, $L_2 = 0.7$ nH, and $C_2 = 0.7$ pF. In the simulation, the lumped components L_2 and C_2 are raised by 0.5 mm and connected to the microstrip lines by two metal plates to avoid overlapping. Considering the losses in the actual lumped components, all the lumped components are connected in series with a 0.5-Ω resistor. The diameters of feeding pins d_p are increased to 1 mm for ease of soldering.

B. Simulated and Measurement Results

Fig. 12 shows the simulated complex magnitude current distributions at 2.45 GHz with different excitations. Due to symmetry, only the current distribution with the excitation of ports 1 and 2 is presented for brevity. When one port is excited, current nulls will appear on other loaded ports, which means that good isolation is achieved. The current nulls are generated by the cancellation of the coupling from the antenna branch and the coupling from the decoupling structure.

To validate the performance of the proposed antenna, a prototype is fabricated and measured. The photograph of the proposed antenna is presented in Fig. 13. Three semi-rigid

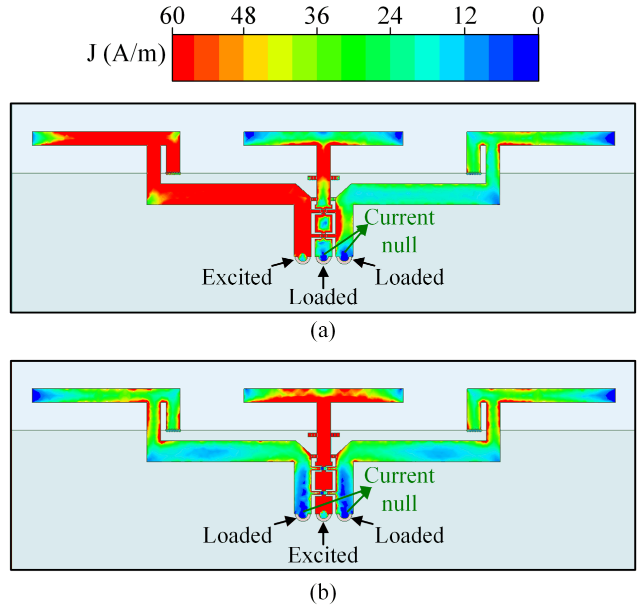

Fig. 12. Simulated complex magnitude current distribution of the proposed antenna at 2.45 GHz with (a) port 1 excited and other ports loaded and (b) port 2 excited and other ports loaded.

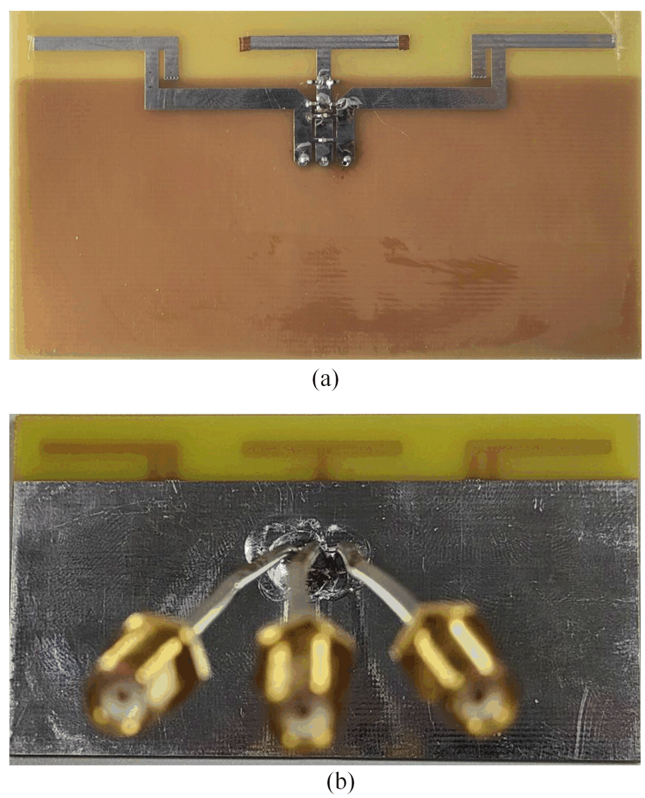

Fig. 13. Photograph of the fabricated antenna. (a) Top view. (b) Bottom view.

coaxial cables are used to feed the antenna. The inner conductors are connected to the coupled three-line and the outer conductors are soldered to the ground. Due to fabrication errors, we fine-tuned the dimensions of the antenna branch, as shown in Fig. 13(a). The simulated and measured S-parameters are presented in Fig. 14. In comparison to Ant V, the increased diameter of the feeding pin of the proposed

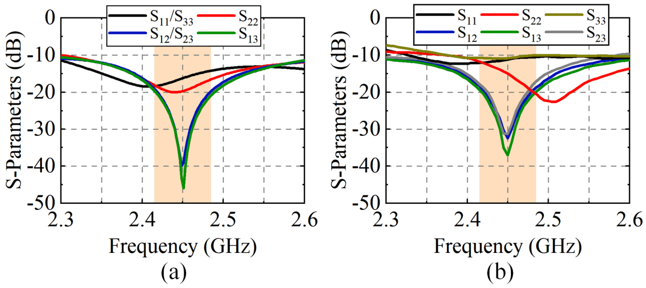

Fig. 14. (a) Simulated and (b) measured S-parameters.

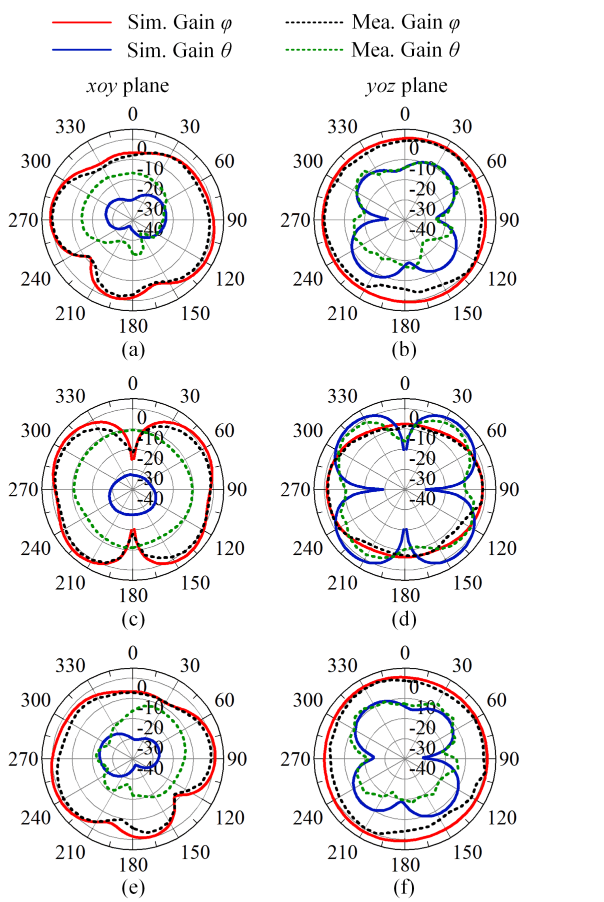

Fig. 15. Simulated and measured radiation patterns at 2.45 GHz. (a) Port 1, (c) port 2, and (e) port 3 in the *xoy* plane. (b) Port 1, (d) port 2, and (f) port 3 in the *yoz* plane.

antenna alters the impedance matching slightly while having little influence on the isolation. The reason is that after good isolation is attained, the three antennas are independent of each other. The measured results show that a peak isolation of 37 dB is realized between ports 1 and 3. The measured peak isolation between any two ports is higher than 31 dB. In the lower band of wireless fidelity (Wi-Fi) from 2.415 to 2.485 GHz, the isolation is higher than 17 dB. The little deviation can be attributed to errors in the lumped components and fabrication. In general, the measured S-parameters accord well with the simulated results.

Fig. 15 presents the simulated and measured radiation patterns with different port excitations in the *xoy* plane and *yoz* plane at 2.45 GHz. Due to the symmetry of the antennas,

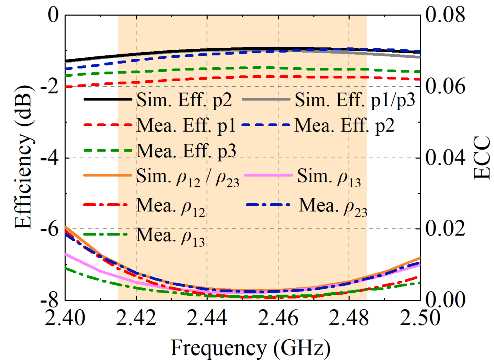

Fig. 16. Simulated and measured efficiencies and ECCs.

the radiation patterns of ports 1 and 3 are symmetrical and complementary. In the *xoy* plane, the measured gain θ is higher than the simulated results. The deviation is introduced by the traveling-wave current generated on the outside surface of the feeding cable. The gain fluctuations near 180° shown in Fig. 15(b), (d), and (f) are due to the obstruction of the long feeding line in the chamber. When the rotating platform is rotated to 180°, the feeding line appears between the antenna under test and the transmitting antenna, which results in errors in the gain measurement. Generally, the measured results agree well with the simulated results.

To evaluate the diversity and radiation performance of the proposed antenna, the envelope correlation coefficients (ECCs) and efficiencies are illustrated in Fig. 16. The ECCs between the ports are calculated by simulated and measured far-field radiation patterns [29]. As shown in Fig. 16, the measured ECCs between any two ports are lower than 0.01 in the desired band, demonstrating good diversity performance of the proposed MIMO antenna. The measured efficiency is 0.8 dB lower than the simulated efficiency due to the higher loss of the actual substrate and lumped components. The measured efficiencies of the three ports are higher than −1.9 dB (64.4%) in the desired band. Different from the simulated results, the measured efficiencies under different port excitations are different even for the symmetric ports. The deviations in the measured efficiencies can be attributed to the traveling-wave current and the obstruction effect of the feeding line. On the one hand, the symmetry of the antenna is destroyed due to the presence of the feeding line. On the other hand, for antennas with different gains in the backside direction, the errors in radiation pattern and efficiency introduced by the obstruction of the feeding line are different. Therefore, deviations occur in the efficiency measurement for different ports.

V. Discussion and Comparison

A. Influence of the Spacing on Isolation

To investigate the effect of the antenna spacing on the decoupling performance, the proposed method is applied to three IFAs with a reduced spacing d_7 of only 1.2 mm ($\sim 0.01\lambda_0$). The configuration and detailed dimensions are displayed in Fig. 17. As analyzed above, when three active impedances $Z_{11,\mathrm{M1}}$, $Z_{11,\mathrm{M2}}$, and $Z_{11,\mathrm{M3}}$ are all perfectly matched, perfect impedance matching of ports 1 and 3 and

TABLE II
COMPARISON AMONG THE DECOUPLING OF COLLINEAR THREE ANTENNAS

Reference	Decoupling scheme	Numerous iteration and optimization	Bandwidth	Distance	Isolation	Efficiency
[8]	Neutralization line	Yes	3.3%	0.12 λ_0	>20dB	>80%
[23]	Decoupling circuit	No	1.25%	0.16 λ_0	>25 dB	>70%
[24]	Transmission line with Branch	Yes	2.9%	0.12 λ_0	>13 dB	N.G.
[25]	Dummy element	Yes	1.1%	0.14 λ_0	>28 dB	>50%
[26]	Self-decoupled	Yes	5.7%	0 λ_0*	>11 dB	>51%
This work	Coupled three-line & Lumped components	No	2.9%	0.07 λ_0	>17dB	>64%

*: Shared radiator design is used in this work.
Distance: the spacing from edge to edge of the adjacent elements. Isolation: considering both |S21| and |S31| in the desired band. λ_0: free-space wavelength at the center frequency.

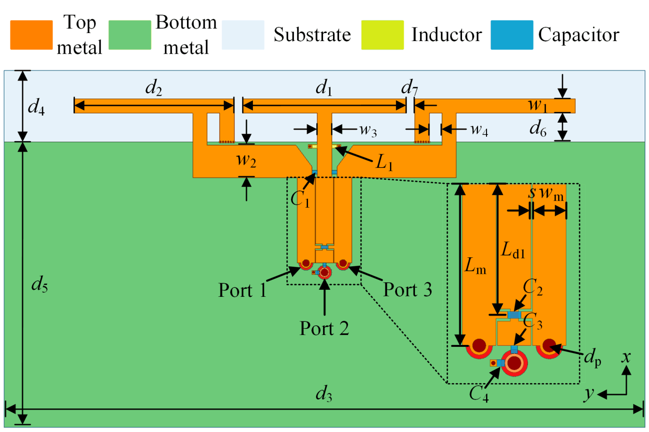

Fig. 17. Configuration of the decoupling design with a smaller spacing. The detailed dimensions are $d_1 = 23.04$, $d_2 = 22.5$, $d_3 = 90$, $d_4 = 10$, $d_5 = 40$, $d_6 = 4$, $d_7 = 1.2$, $w_1 = 2$, $w_2 = 4.5$, $w_3 = 2$, $w_4 = 1.8$, $L_m = 7.5$, $L_{d1} = 9.75$, $s = 0.1$, $L_{m1} = 12$, and $d_p = 1$, all in millimeters. The value of lumped components are $L_1 = 1.6$ nH, $C_1 = 2$ pF, $C_2 = 1$ pF, $C_3 = 6$ pF, and $C_4 = 1$ pF.

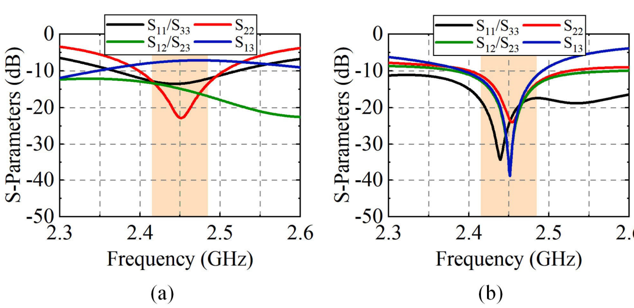

Fig. 18. Simulated S-parameters of the IFAs with a smaller spacing. (a) Without decoupling structure (reference). (b) With decoupling structure.

perfect isolation will be attained. The condition of active impedance matching does not guarantee impedance matching of port 2. In the case with a smaller spacing, port 2 is not matched after isolation is achieved. Therefore, as shown in Fig. 17, a series capacitor C_3 and a parallel capacitor C_4 are added to port 2 for impedance matching. The simulated S-parameters of the three IFAs with and without the decoupling structure are presented in Fig. 18. The peak isolation

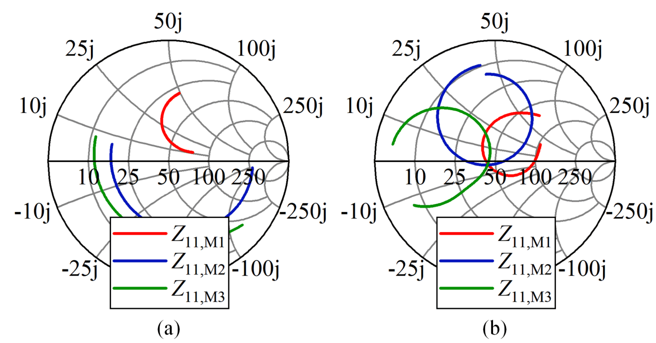

Fig. 19. Simulated S-parameters of the IFAs with a smaller spacing. (a) Without decoupling structure (reference). (b) With decoupling structure.

between the adjacent elements is enhanced from 7 to 36 dB and the peak isolation between the nonadjacent elements is enhanced from 13 to 39 dB. The decoupling bandwidth is inevitably reduced due to the worse initial isolation between the antennas in the case of reduced spacing. In the desired band from 2.415 to 2.485 GHz, the isolation between the adjacent elements is better than 12 dB and the isolation between the nonadjacent elements is better than 13 dB. As illustrated in Fig. 19(a), due to high mutual coupling between the elements, the three impedance loci of the reference antenna without decoupling structure are far away from each other on the Smith chart. As displayed in Fig. 19(b), with the decoupling structure, the three impedance loci intersect near the matching point, which implies that good isolation is attained. In sum, with smaller element spacing, the decoupling bandwidth will be narrow, but the proposed decoupling method is still able to provide good decoupling performance.

B. Comparison

To demonstrate the advantages of the proposed antenna, Table II presents a comparison between our decoupling method and other decoupling schemes. The decoupling designs in [8], [24], [25], and [26] involve multiple iterations of simulation and optimization, which makes the decoupling process complex and time-consuming. Although repeated iterative simulation and optimization are not required in [23], decoupling can only be achieved between adjacent antennas. The decoupling between nonadjacent elements is limited to specific spacing. Compared to previous works, our work achieves considerable isolation between any two antennas with a small distance. Moreover, our approach transforms the decoupling problem into the active impedance matching problem, which can be tackled in a simple step-by-step manner without the need for repeated optimization. The design provides new insights into the intricate problem of decoupling multiple antennas.

VI. Conclusion

This work introduces a systematic decoupling solution for axial symmetric three antennas. The active S-parameters with different simultaneous excitation modes are proposed for decoupling design. Leveraging the analysis of active S-parameters, the decoupling problem can be simplified to the problem of active impedance matching. Once all three active impedances under different excitations are matched, decoupling is achieved. Utilizing the coupled three-line and lumped components, active impedance matching can be accomplished in steps. Three axial symmetric IFAs are presented as an example and good isolation performance is achieved. The proposed decoupling scheme offers a physical insight into the decoupling process for axial symmetric three MIMO antennas, which helps to solve the decoupling problem intuitively and efficiently.

References

[1] S. Ghosh, T. N. Tran, and T. Le-Ngoc, “Dual-layer EBG-based miniaturized multi-element antenna for MIMO systems,” *IEEE Trans. Antennas Propag.*, vol. 62, no. 8, pp. 3985–3997, Aug. 2014.

[2] X. Yang, Y. Liu, Y. Xu, and S. Gong, “Isolation enhancement in patch antenna array with fractal UC-EBG structure and cross slot,” *IEEE Antennas Wireless Propag. Lett.*, vol. 16, pp. 2175–2178, 2017.

[3] X. Tan, W. Wang, Y. Wu, Y. Liu, and A. A. Kishk, “Enhancing isolation in dual-band meander-line multiple antenna by employing split EBG structure,” *IEEE Trans. Antennas Propag.*, vol. 67, no. 4, pp. 2769–2774, Apr. 2019.

[4] E. Rajo-Iglesias, Ó. Quevedo-Teruel, and L. Inclan-Sanchez, “Mutual coupling reduction in patch antenna arrays by using a planar EBG structure and a multilayer dielectric substrate,” *IEEE Trans. Antennas Propag.*, vol. 56, no. 6, pp. 1648–1655, Jun. 2008.

[5] B. Qian, X. Chen, L. Zhao, J. Chen, and A. A. Kishk, “Reduced cross-polarization and backside radiations for rectangular microstrip antennas using defected ground structure combined with decoupling structure,” *IEEE Antennas Wireless Propag. Lett.*, vol. 22, pp. 517–521, 2023.

[6] Y. Wang and Z. Du, “A wideband printed dual-antenna system with a novel neutralization line for mobile terminals,” *IEEE Antennas Wireless Propag. Lett.*, vol. 12, pp. 1428–1431, 2013.

[7] Y. Wang and Z. Du, “A wideband printed dual-antenna with three neutralization lines for mobile terminals,” *IEEE Trans. Antennas Propag.*, vol. 62, no. 3, pp. 1495–1500, Mar. 2014.

[8] M. Li, L. Jiang, and K. L. Yeung, “A general and systematic method to design neutralization lines for isolation enhancement in MIMO antenna arrays,” *IEEE Trans. Veh. Technol.*, vol. 69, no. 6, pp. 6242–6253, Jun. 2020.

[9] T. Pei, L. Zhu, J. Wang, and W. Wu, “A low-profile decoupling structure for mutual coupling suppression in MIMO patch antenna,” *IEEE Trans. Antennas Propag.*, vol. 69, no. 10, pp. 6145–6153, Oct. 2021.

[10] A. Zhang, K. Wei, Q. Guan, and Y. Hu, “Compactly placed high-isolated antenna pair with independent control of decoupling amplitude and phase,” *IEEE Trans. Antennas Propag.*, vol. 71, no. 3, pp. 2814–2819, Mar. 2023.

[11] S.-W. Su, C.-T. Lee, and Y.-W. Hsiao, “Compact two-inverted-F-antenna system with highly integrated π-shaped decoupling structure,” *IEEE Trans. Antennas Propag.*, vol. 67, no. 9, pp. 6182–6186, Sep. 2019.

[12] F. Liu, J. Guo, L. Zhao, G. Huang, Y. Li, and Y. Yin, “Dual-band metasurface-based decoupling method for two closely packed dual-band antennas,” *IEEE Trans. Antennas Propag.*, vol. 68, no. 1, pp. 552–557, Jan. 2020.

[13] G. Zhao, T. Liu, J. Jiang, L. Zhao, G.-L. Huang, and W. Lin, “Polarization selective partial reflective decoupling layers for mutual coupling reduction of two closely spaced dual-polarized antennas,” *IEEE Trans. Antennas Propag.*, vol. 70, no. 11, pp. 11205–11210, Nov. 2022.

[14] B. Liu, X. Chen, J. Tang, A. Zhang, and A. A. Kishk, “Co- and cross-polarization decoupling structure with polarization rotation property between linearly polarized dipole antennas with application to decoupling of circularly polarized antennas,” *IEEE Trans. Antennas Propag.*, vol. 70, no. 1, pp. 702–707, Jan. 2022.

[15] A. Zhang, K. Wei, and Z. Zhang, “Multiband and wideband self-multipath decoupled antenna pairs,” *IEEE Trans. Antennas Propag.*, vol. 71, no. 7, pp. 5605–5615, Jul. 2023.

[16] X. Tian and Z. Du, “Wideband shared-radiator four-element MIMO antenna module for 5G mobile terminals,” *IEEE Trans. Antennas Propag.*, vol. 71, no. 6, pp. 4799–4811, Jun. 2023.

[17] Y. He and Y. Li, “Compact co-linearly polarized microstrip antenna with fence-strip resonator loading for in-band full-duplex systems,” *IEEE Trans. Antennas Propag.*, vol. 69, no. 11, pp. 7125–7133, Nov. 2021.

[18] L. Sun, Y. Li, Z. Zhang, and H. Wang, “Antenna decoupling by common and differential modes cancellation,” *IEEE Trans. Antennas Propag.*, vol. 69, no. 2, pp. 672–682, Feb. 2021.

[19] L. Sun, Y. Li, and Z. Zhang, “Decoupling between extremely closely spaced patch antennas by mode cancellation method,” *IEEE Trans. Antennas Propag.*, vol. 69, no. 6, pp. 3074–3083, Jun. 2021.

[20] J. Hu, W. Zhang, Y. Li, and Z. Zhang, “Compact co-polarized PIFAs for full-duplex application based on CM/DM cancellation theory,” *IEEE Trans. Antennas Propag.*, vol. 69, no. 11, pp. 7103–7110, Nov. 2021.

[21] A. Zhang, K. Wei, Y. Hu, and Q. Guan, “High-isolated coupling-grounded patch antenna pair with shared radiator for the application of 5G mobile terminals,” *IEEE Trans. Antennas Propag.*, vol. 70, no. 9, pp. 7896–7904, Apr. 2022.

[22] Z. Zhou, Y. Ge, J. Yuan, Z. Xu, and Z. D. Chen, “Wideband MIMO antennas with enhanced isolation using coupled CPW transmission lines,” *IEEE Trans. Antennas Propag.*, vol. 71, no. 2, pp. 1414–1423, Feb. 2023.

[23] M. Li, L. Jiang, and K. L. Yeung, “Novel and efficient parasitic decoupling network for closely coupled antennas,” *IEEE Trans. Antennas Propag.*, vol. 67, no. 6, pp. 3574–3585, Jun. 2019.

[24] Y.-F. Cheng and K.-K. M. Cheng, “A novel and simple decoupling method for a three-element antenna array,” *IEEE Antennas Wireless Propag. Lett.*, vol. 16, pp. 1072–1075, 2017.

[25] J.-Y. Deng, J.-Y. Li, and L.-X. Guo, “Decoupling of a three-port MIMO antenna with different impedances using reactively loaded dummy elements,” *IEEE Antennas Wireless Propag. Lett.*, vol. 17, pp. 430–433, 2018.

[26] B. Yang, Y. Xu, J. Tong, Y. Zhang, Y. Feng, and Y. Hu, “Tri-port antenna with shared radiator and self-decoupling characteristic for 5G smartphone application,” *IEEE Trans. Antennas Propag.*, vol. 70, no. 6, pp. 4836–4841, Jun. 2022.

[27] D. M. Pozar, “A relation between the active input impedance and the active element pattern of a phased array,” *IEEE Trans. Antennas Propag.*, vol. 51, no. 9, pp. 2486–2489, Sep. 2003.

[28] D. Pavlidis and H. L. Hartnagel, “The design and performance of three-line microstrip couplers,” *IEEE Trans. Microw. Theory Techn.*, vol. MTT-24, no. 10, pp. 631–640, Oct. 1976.

[29] R. G. Vaughan and J. B. Andersen, “Antenna diversity in mobile communications,” *IEEE Trans. Veh. Technol.*, vol. VT-36, no. 4, pp. 147–172, Nov. 1987.

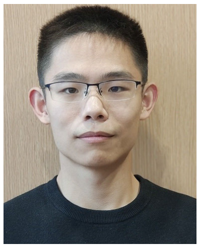

Zhongyao Cao (Graduate Student Member, IEEE) received the B.S. degree from the University of Electronic Science and Technology of China, Chengdu, China, in 2020. He is currently pursuing the Ph.D. degree in electrical engineering with Tsinghua University, Beijing, China.

His current research interests include reconfigurable antennas, beam scanning arrays, and reflectarray antennas.

Le Chang (Senior Member, IEEE) received the B.S. degree in electronics and information engineering from Xidian University, Xi'an, China, in 2012, and the Ph.D. degree in electrical engineering from Tsinghua University, Beijing, China, in 2017.

In July 2017, he joined Huawei Technology Ltd., Beijing, as a Senior Antenna Engineer. Since 2021, he has been with Xi'an Jiaotong University, Xi'an, where he is currently an Associate Professor. He has authored or co-authored 45 journal articles. His current research interests include mobile antennas and mmW/THz antennas.

Yue Li (Senior Member, IEEE) received the B.S. degree in telecommunication engineering from Zhejiang University, Hangzhou, Zhejiang, China, in 2007, and the Ph.D. degree in electronic engineering from Tsinghua University, Beijing, China, in 2012.

In June 2012, he was a Post-Doctoral Fellow with the Department of Electronic Engineering, Tsinghua University. In December 2013, he was a Research Scholar with the Department of Electrical and Systems Engineering, University of Pennsylvania, Philadelphia, PA, USA. He was also a Visiting Scholar with the Institute for Infocomm Research (I2R), A∗STAR, Singapore, in 2010, and Hawaii Center of Advanced Communication (HCAC), University of Hawaii at Manoa, Honolulu, HI, USA, in 2012. Since January 2016, he has been with Tsinghua University, where he is currently an Assistant Professor and an Associate Professor with the Department of Electronic Engineering. He has authored and co-authored over 210 journal articles and 50 international conference papers. He holds 26 granted Chinese patents. His current research interests include metamaterials, plasmonics, electromagnetics, nanocircuits, mobile and handset antennas, MIMO and diversity antennas, and millimeter-wave antennas and arrays.

Dr. Li was a recipient of the the Principal Scholarship of Tsinghua University in 2011, the Outstanding Doctoral Dissertation of Beijing Municipality in 2013, the URSI General Assembly and Scientific Symposium (GASS) in 2014, the Asia–Pacific Radio Science Conference (AP-RASC) in 2016, the International Symposium on Electromagnetic Theory (EMTS) in 2016, the International Conference on Microwave and Millimeter Wave Technology (ICMMT) in 2016 and 2020, the International Symposium on Antennas, Propagation and EM Theory (ISAPE) in 2016 and 2021, the Issac Koga Gold Medal from URSI General Assembly in 2017, the Second Prize of Science and Technology Award of China Institute of Communications in 2017, the National Conference on Microwave and Millimeter Waves (NCMMW) in 2017 and 2018, the National Conference on Antennas (NCANT) in 2017 and 2019, the Asia–Pacific Conference on Antennas and Propagation (APCAP) in 2017 and 2020, the International Applied Computational Electromagnetics Society Symposium (ACES) in 2018, the Atlantic Radio Science Conference (AT-RASC) in 2018, the Cross Strait Quad-Regional Radio Science and Wireless Technology Conference (CSQRWC) in 2018, the Young Scientist Award from the Conferences of Progress in Electromagnetics Research Symposium (PIERS) in 2019, the International Symposium on Antennas and Propagation (ISAP) in 2019, U.K.–Europe–China Workshop on Millimeter Waves and Terahertz Technologies (UCMMT) in 2020, the Best Paper Award from the conferences of PhotonIcs and Electromagnetics Research Symposium (PIERS) in 2021, and the International Workshop on Electromagnetics (iWEM) in 2021. He is serving as an Associate Editor for IEEE Transactions on Antennas and Propagation, IEEE Antennas and Wireless Propagation Letters, *Microwave and Optical Technology Letters*, and *Computer Applications in Engineering Education*. He is also serving on the Editorial Board of *Scientific Reports, Sensors, and Electronics*.

Kunpeng Wei (Senior Member, IEEE) received the B.S. degree in electronic and information engineering from the Huazhong University of Science and Technology, Wuhan, China, in 2008, and the Ph.D. degree in electrical engineering from Tsinghua University, Beijing, China, in 2013.

In 2012, he was a Visiting Scholar with the School of Electrical and Computer Engineering, Georgia Institute of Technology, Atlanta, GA, USA. From July 2013 to December 2015, he was employed with the Radar Research Institute, Chinese Air Force Research Laboratory, Beijing, conducting research in the areas of phased-array antenna design and radar system design. He joined the Consume Business Group, Huawei Inc., Xi'an, China, in 2016, where he was an Antenna Specialist and the Director of Xi'an Antenna Team. In 2021, he joined Honor Device Company Ltd., Beijing, when this company split from Huawei, and he was the Director of the Honor Antenna Team. After leaving Honor, he joined Xiaomi Corporation, Beijing, in 2023. He is currently the Chief Antenna Expert and the Head of the Antenna Technology Team. He leads a large group of antenna experts and engineers and takes full responsibility for the research of antenna technologies to guarantee the market success of all Xiaomi's products ranging from smartphones, electric cars, tablets, and other IOT devices. He is a special-level external expert of China Academy of Information and Communications Technology. He is also an Adjunct Professor with the School of Electronics and Information Engineering, Shenzhen University, Shenzhen, China. He has authored over referred 60 articles on consumer electronics antenna design. He holds over 100 granted U.S./European/Japanese/Chinese patents and has other more than 20 patent applications in pending. His current research interests include MIMO antenna technology, satellite communication technology, 5.5G/millimeter wave technology, UWB wireless technology, and meta-antennas for "Human × Car × Home" smart ecosystem.

Dr. Wei is an IET Fellow. He was a recipient of the Principal Scholarship of Tsinghua University in 2012, the Huawei Team Gold Medal Award in 2017, the Huawei Individual Gold Medal Award in 2018, and the Honor Team Gold Medal Award in 2021. He has been serving as an Associate Editor for *IET Electronics Letters* since October 2021 and IEEE Open Journal of Antennas and Propagation since October 2023.

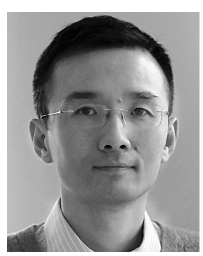

Zhijun Zhang (Fellow, IEEE) received the B.S. and M.S. degrees from the University of Electronic Science and Technology of China, Chengdu, China, in 1992 and 1995, respectively, and the Ph.D. degree from Tsinghua University, Beijing, China, in 1999.

In 1999, he was a Post-Doctoral Fellow with the Department of Electrical Engineering, University of Utah, Salt Lake City, UT, USA, where he was appointed as a Research Assistant Professor in 2001. In May 2002, he was an Assistant Researcher with the University of Hawaii at Manoa, Honolulu, HI, USA. In November 2002, he joined Amphenol T&M Antennas, Vernon Hills, IL, USA, as a Senior Staff Antenna Development Engineer and was then promoted to the position of Antenna Engineer Manager. In 2004, he joined Nokia Inc., San Diego, CA, USA, as a Senior Antenna Design Engineer. In 2006, he joined Apple Inc., Cupertino, CA, USA, as a Senior Antenna Design Engineer and was then promoted to the position of Principal Antenna Engineer. Since August 2007, he has been with Tsinghua University, where he is currently a Professor with the Department of Electronic Engineering. He is the author of *Antenna Design for Mobile Devices* (Wiley, First Edition 2011, Second Edition 2017).

Dr. Zhang served as an Associate Editor for IEEE Transactions on Antennas and Propagation from 2010 to 2014 and IEEE Antennas and Wireless Propagation Letters from 2009 to 2015.